Slip flow in triangular and trapezoidal microchannels

Jeerasak Pitakarnnop, Sandrine Geoffroy, Stéphane Colin, Lucien Baldas

SLIP FLOW IN TRIANGULAR AND TRAPEZOIDAL MICROCHANNELS

Jeerasak Pitakarnnop*, Sandrine Geoffroy*, Stéphane Colin*, Lucien Baldas*

* LGMT-INSA, 135 avenue de Rangueil, 31077 Toulouse cedex 4, France

ABSTRACT

Modeling gaseous slip flows in microchannels is now possible by means of commercial CFD codes such as Fluent. This article shows that the so-called Low Pressure Boundary Slip method proposed in Fluent for implementing slip conditions leads to inaccurate results concerning velocity at the walls, particularly in angles such as those met in microchannels with triangular or trapezoidal sections. We propose another method whose aim is to avoid this issue. Numerical results are compared for validation to the analytical solution obtained for an equilateral triangular section. Finally, the method is applied to isosceles triangular and trapezoidal sections of practical interest, since they are frequently etched in silicon microsystems.

1. INTRODUCTION

The slip flow regime is a slightly rarefied regime of great interest for gas flows through microchannels [1]. It typically corresponds to a Knudsen number between 10^{-3} and 10^{-1}, and this range is commonly reached in standard conditions for hydraulic diameters in the order of a few micrometers. The Knudsen layer plays a fundamental role in the slip flow regime. This thin layer, one or two molecular mean free paths in thickness, is a region of local non-equilibrium which is observed in any gas flow near a surface. In non rarefied flows, the Knudsen layer is too thin for having any significant influence, but in the slip flow regime, it should be taken into account.

Although the Navier-Stokes equations are not valid in the Knudsen layer, due to a nonlinear stress/strain-rate behavior in this small layer [2], their use with appropriate boundary velocity slip and temperature jump conditions proved to be accurate for predicting mass flow rates [3],[4] and velocity profiles out of the Knudsen layer. Classically, the real flow is not simulated within the Knudsen layer, but the influence of the Knudsen layer on the flow outside this non-equilibrium layer is taken into account, replacing the no-slip condition at the wall with a slip-flow condition. The first slip-flow condition was proposed by Maxwell [5] and reduces to the form

$$W_{slip} = W_s - W_w = \frac{2-\sigma_v}{\sigma_v} A_\alpha \lambda \left.\frac{\partial W}{\partial n}\right|_{wall} \qquad (1)$$

if isothermal flow is assumed. In this equation, W_{slip} is the slip velocity, W_s is the flow velocity at the wall and W_w is the velocity of the wall, the normal direction of which is noted n. The mean free path of the molecules is λ and σ_v is the tangential momentum accommodation coefficient, equal to unity for perfectly diffuse molecular reflection and zero for purely specular reflection. In Maxwell's model, the dimensionless coefficient A_α was taken equal to unity, which overestimates the real velocity at the wall but leads to a rather good prediction of the velocity out of the Knudsen layer. Cercignani has shown [6] that a better prediction of the flow out of the Knudsen layer would be obtained with $A_\alpha = 1.146$. Equation (1) is called first-order slip boundary condition, because it involves the Knudsen number Kn (ratio of the mean free path λ over a reference length) and the first derivative $\left.\partial W/\partial n\right|_{wall}$. Second-order boundary conditions involving Kn^2 and second derivative $\left.\partial^2 W/\partial n^2\right|_{wall}$ have been further proposed in the attempt to predict flow rates with improved accuracy [1], [7], [8], [9], [10], [11].

For benchmark flows such as Poiseuille or Couette flows in microchannels with simple constant section (plane, circular, rectangular), isothermal slip flow may be analytically modeled [12], [13], even with second-order boundary conditions [14] such as those proposed by Deissler. However, for other sections such as isosceles triangular or trapezoidal sections, frequently met in microchannels fabricated by silicon wet etching, numerical simulations are required.

The aim of this paper is to analyze possibilities of slip flow simulations with the commercial CFD code Fluent. Rarefied gas flow simulation is feasible in Fluent using the "Low Pressure Boundary Slip" (LPBS) option in the "Viscous Model" panel. However, the choice of velocity slip boundary condition is limited to Maxwell's first order model with an expression of the mean free path adjustable via the value of the Lennard-Jones length. Moreover, we show in this article that the LPBS method is inaccurate for predicting slip near the corners of the section, leading to significant errors in flow rate estimation. In order to overcome these issues, we propose another method which uses "Moving Wall" (MW) boundary conditions. Comparison of both models is first made with the only triangular section for which an analytical solution of Poiseuille slip flow is available: the equilateral triangular section. After validation of the proposed method, slip flow in isosceles triangular and trapezoidal sections is simulated and data are discussed.

2. SLIP FLOW IN AN EQUILATERAL TRIANGULAR SECTION

The Cartesian coordinates system (x, y, z) is used. Each side of the equilateral triangular section has a length of $2\sqrt{3}L$, so that $x \in [-2L; L]$ and $y \in [-\sqrt{3}L; \sqrt{3}L]$.

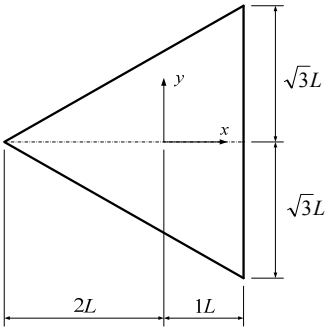

Figure 1: Equilateral triangular section.

2.1 Analytical solution

For a locally fully developed gas flow in a cylindrical (i.e. straight and with constant section) microchannel, the momentum equation reduces to the Poisson equation

$$\frac{\partial^2 W}{\partial x^2} + \frac{\partial^2 W}{\partial y^2} = \frac{1}{\mu}\frac{dP}{dz}, \tag{2}$$

which can be written in a non-dimensional form as

$$\nabla^2 W^* = \frac{\partial^2 W^*}{\partial x^{*2}} + \frac{\partial^2 W^*}{\partial y^{*2}} = -1, \tag{3}$$

with

$$x^* = x/L \; ; \; y^* = y/L \; ; \; W^* = W/W_0 \; . \tag{4}$$

In these equations, W is the streamwise velocity,

$$W_0 = -\frac{L^2}{\mu}\frac{dP}{dz}, \tag{5}$$

P is the pressure and μ is the dynamic viscosity of the gas. The Knudsen number, which quantifies rarefaction effects, is defined as

$$Kn = \frac{\lambda}{D_h} \tag{6}$$

where the hydraulic diameter D_h = $2L$ for an equilateral triangular section. Solving Equation (3) with the boundary conditions

$$W^*_{slip} = \alpha^* \left.\frac{\partial W^*}{\partial n^*}\right|_{wall}, \tag{7}$$

where $n^* = n/L$ and the dimensionless slip coefficient $\alpha^* = \alpha/L$ with $\alpha = 2\left[(2-\sigma_v)/\sigma_v\right] A_\alpha \lambda$, leads to [15]

$$W^* = -\frac{1}{4}\left(x^{*2} + y^{*2}\right) + A^* + B^*\left(x^{*3} - 3x^* y^{*2}\right), \tag{8}$$

where

$$A^* = \frac{2 + 6\alpha^* + 3\alpha^{*2}}{6\left(1+\alpha^*\right)} \; ; \; B^* = \frac{-1}{12\left(1+\alpha^*\right)}. \tag{9}$$

The mass flow rate

$$\dot{m} = -\frac{3\sqrt{3}L^3\left(3L^2 + 15L\alpha + 10\alpha^2\right)}{20\left(L+\alpha\right)}\frac{\rho}{\mu}\frac{dP}{dz}, \tag{10}$$

which leads to the classic no-slip value

$$\dot{m}_{ns} = -\frac{9\sqrt{3}L^4}{20}\frac{\rho}{\mu}\frac{dP}{dz} \tag{11}$$

when $\alpha = 0$, and to the non-dimensional flow rate

$$\dot{m}^* = \frac{\dot{m}}{\dot{m}_{ns}} = \frac{\left(3 + 15\alpha^* + 10\alpha^{*2}\right)}{3\left(1+\alpha^*\right)}. \tag{12}$$

2.2 Numerical simulation

Calculation domains and 3-D grids are generated with Gambit, the Fluent's preprocessing software. Two types of domains are simulated according to the considered symmetries:

a) the first one is a sixth of the section (S/6), which can be used only for the equilateral section (figure 2a),
b) the second one is a half of the section (S/2) (figure 2b).

Grids are created with a reasonable cells density: 8319 and 20038 quadrilateral cells for one sixth (S/6) and one half (S/2) of the section respectively. These grids are refined near boundaries to improve the velocity gradients calculations.

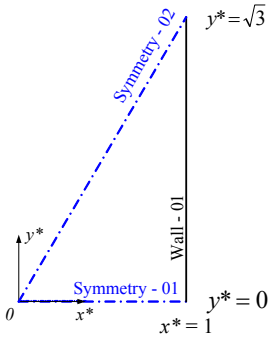

Figure 2a: simulation on one sixth of a section (S/6)

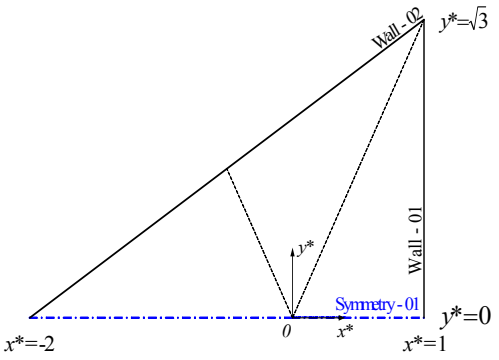

Figure 2 b: simulation on one half section (S/2)

Simulations are performed for a nitrogen gas flow. Periodic boundary conditions are used to model incompressible locally fully developed isothermal flow. The effect of the number of cells along the z-direction has been tested, showing no particular consequence on the results. Consequently, only one cell along the z-direction has been used afterwards. The laminar viscous model is selected. Double precision calculations are done with second order discretization scheme for a better accuracy.

The aim of this paper is to validate and to determine advantages and drawbacks of two methods to process slip velocity boundary conditions:

(l) The first one uses the so-called Low Pressure Boundary Slip (LPBS) condition which can be simply applied by selecting it in Fluent's "Viscous Model" menu.

(2) The second method is the one that we propose in this article: it is an iterative method that we called Moving Wall (MW) method. Indeed, several treatments are required. The simulation is first done with no slip conditions. Results of this preliminary step are used to calculate slip flow velocities at the wall by using equation (7). These local slip velocities are then applied to each cell at the wall as a moving wall boundary condition. For 2-D flows between parallel plates, this first iteration is sufficient, since in this case the transverse velocity gradient at the wall is the same with or without slip at the wall [12]. In 3-D flows through an equilateral section, further iterations are needed: for each iteration, the slip velocity is calculated from the previous iteration by using equation (7) with the help of Fluent's Custom Field Function and iterations are done until the slip velocity at the wall is stable. However, to improve the accuracy of the results near boundaries, especially in acute angles, slip velocities are extrapolated outside Fluent and the calculated results are applied to MW boundaries cell by cell. In each tested configuration the same grid is used for both methods. Moreover, the two methods are based on the resolution of the same set of equations (cf. 2.1.), the only difference being the way to implement the slip boundary condition at the wall.

For a valid comparison between both methods, the mean free path used for the MW method is defined as it is with Fluent's LPBS method, that is

$$\lambda = \frac{k_B T}{\sqrt{2}\pi\sigma^2 P}, \tag{13}$$

Where $k_B = 1.38066 \times 10^{-23}\ \mathrm{J\,K^{-1}}$ is the Boltzmann constant, T the temperature, P the pressure and σ the Lennard-Jones characteristic length of the gas. Any other kind of expression for λ, for example based on hard spheres (HS), variable hard spheres (VHS) or variable soft spheres (VSS) models, could be used in the MW method. Note also that only Maxwell's first order slip velocity model can be used with LPBS conditions. Thus, in order to adequately compare both methods, only this kind of boundary has been used here for the MW method, which is nevertheless valid with higher-order boundary conditions. Moreover, the slip coefficient

$$\alpha = \frac{2-\sigma_v}{\sigma_v} A_\alpha \lambda \tag{14}$$

is limited with the LPBS method to the Maxwell value $A_\alpha = 1$. The same value has been kept for the MW method.

2.3 Results and discussion

In this article, the accommodation has always been assumed totally diffuse, i.e. with $\sigma_v = 1$, whatever the method, LPBS or MW. The influence of the Knudsen number is firstly investigated. Since Fluent doesn't allow any dimensionless calculation, *Kn* varies according to the operating pressure applied in the calculation domain. To gain calculation time, only one sixth of the section is simulated. The dimensionless mass flow rate results are reported in table 1. To discuss the simulations accuracy, the deviation from the analytical solution is calculated (table 2).

Table 1: Equilateral triangular section – dimensionless mass flow rates for different Knudsen numbers analytical and numerical (S/6) simulations

Kn	$\dot{m}^*$					
	Analytical solution	Fluent No slip	Fluent MW 1st iteration	Fluent MW 2nd iteration	Fluent MW 3rd iteration	Fluent LPBS
0	1.000	0.999				
0.0125	1.100		1.099	1.099	1.099	1.100
0.0500	1.394		1.399	1.392	1.393	1.405
0.0750	1.587		1.599	1.583	1.586	1.611

Concerning no slip simulations, only a 0.059 % deviation from the analytical solution is found (see table 2) and this result is identical for all operating pressures. For slip flow simulations, table 2 shows that the deviation from the analytical solution observed for the MW method is very low (around 0.08 %, the minus sign denoting an underestimation of the flow rate) whatever the Knudsen number. On the other hand, the LPBS method is very accurate for low *Kn*, but this accuracy reduces substantially when *Kn* increases.

Table 2: Equilateral triangular section – flow rate deviation between numerical simulations and analytical solutions

Kn	Flow rate deviation from analytical solution (%)				
	Fluent No slip	Fluent MW 1st iteration	Fluent MW 2nd iteration	Fluent MW 3rd iteration	Fluent LPBS
0	-0.059				
0.0125		-0.029	-0.068	-0.067	0.018
0.0500		0.354	-0.132	-0.085	0.806
0.0750		0.735	-0.226	-0.086	1.537

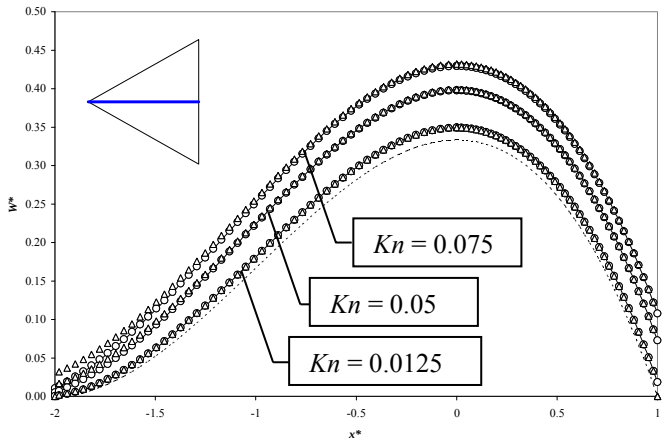

Figure 3: Equilateral triangular section - dimensionless velocity along the symmetry axis ($y^* = 0$); comparison between no slip (--), slip flow analytical results (—), MW (O) and LPBS (Δ) S/6 simulations for different *Kn*

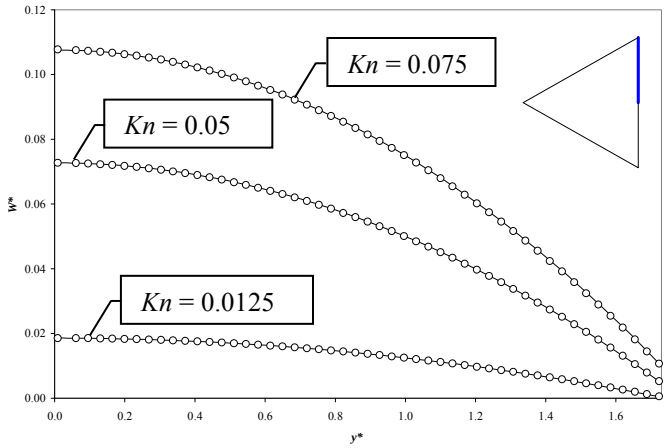

Figure 4: Equilateral triangular section - dimensionless velocity at the wall (*x* = 1*); comparison between analytical solutions (—) and MW (O) S/6 simulations for different *Kn*.

Figures 3, 4 and 5 can give further explanations on this issue. Velocity profiles on the symmetry plane given by both methods are compared in figure 3 to the analytical solutions with slip and no slip assumptions. An excellent agreement can be observed between analytical and numerical results whatever the method for $Kn = 0.0125$. For $Kn = 0.05$ and $Kn = 0.075$, the agreement is still excellent for the MW method but deviations become significant for the LPBS method when approaching the corner at $x^* = 2$. The same excellent agreement is shown in figure 4 between MW and analytical velocity profiles at the wall. As Fluent does not provide directly velocity at the wall when LPBS option is active, velocity profiles have also been plotted in figure 5 at the center of the first cells near the wall for both methods and compared to the analytical solution. In this case, LPBS generates over 100 % deviation at the wall near the corner for high Knudsen numbers, which can explain the lack of precision on the mass flow rate calculation highlighted in table 2.

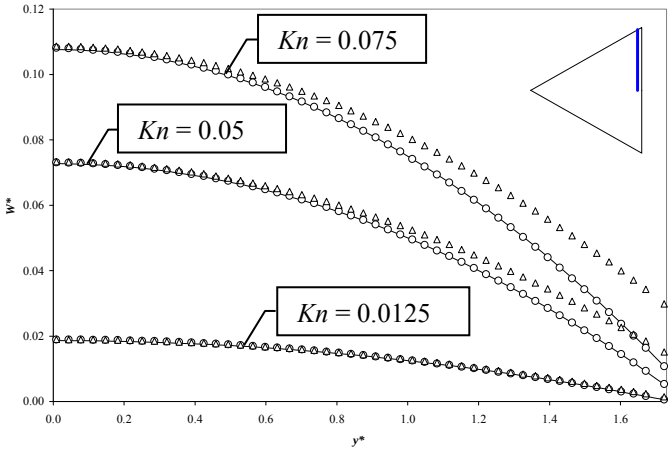

Figure 5: Equilateral triangular section - dimensionless velocity at cells center near the wall ($x^* \approx 1$); comparison between analytical solutions (—), MW (O) and LPBS (Δ) S/6 simulations for different *Kn*

The simulation of one sixth of the section can only be done for an equilateral triangular section. For more complex shapes, obtained for example by wet etching on silicon wafers, only one symmetry plane can be used to reduce the calculation domain. Thus MW and LPBS methods have to be validated on one half of an equilateral triangular section in order to be used for the simulation of more complex channels. For *Kn = 0.075*, the simulated value $\dot{m}^*$ of the dimensionless mass flow rate and its deviation from the analytical value $\dot{m}^*_{ana}$ are shown in table 3, for both methods and a simulation either on one sixth or on one half of the section.

Table 3: Equilateral triangular section - analytical and numerical calculations of mass flow rates calculations from simulations on one sixth (S/6) or one half (S/2) of the section

BC.	Part of the section simulated	*Kn*	$\dot{m}^*$ and deviation ($\frac{\dot{m}^* - \dot{m}^*_{ana}}{\dot{m}^*_{ana}} \times 100$ %)			
			Analytical solution	Fluent 1st iteration	Fluent 2nd iteration	Fluent 3rd iteration
No slip	S/6	0.000	1.000	1.000 (-0.047 %)		
	S/2			1.000 (-0.028 %)		
MW	S/6	0.075	1.587	1.599 (0.735 %)	1.584 (-0.226 %)	1.586 (-0.086 %)
	S/2			1.599 (0.755 %)	1.584 (-0.195 %)	1.585 (-0.160 %)
LPBS	S/6			1.612 (1.537 %)		
	S/2			1.604 (1.035 %)		

The MW method is very slightly less accurate on a half section than on one sixth but the deviation from the analytical solution remains smaller than 0.2 % after the 3rd iteration. The very small difference between S/2 and S/6 simulations could be explained by a 20 % lower grid density for the S/2 simulation. On the other hand, the accuracy of LPBS method is slightly improved with S/2 simulation but still remains much lower than the MW method's one (more than 1 % deviation from the analytical solution). The good prediction of MW method is essentially due to its ability to properly calculate slip in the acute angles, whereas the LPBS method is not accurate there. This is illustrated by figure 6 which represents velocity on the $y^*=0$ symmetry axis. In this figure, S/2 simulation data are directly obtained on the symmetry axis (noted Symmetry-01 in figure 2), and S/6 simulation data are obtained on Symmetry-01 axis for $x \in [0;1]$ and on Symmetry-02 axis for $x \in [-2;0]$. Differences between S/2 and S/6 data remain very low, but the LPBS method largely overestimates the velocity when approaching the corner, at $x^*=-2$.

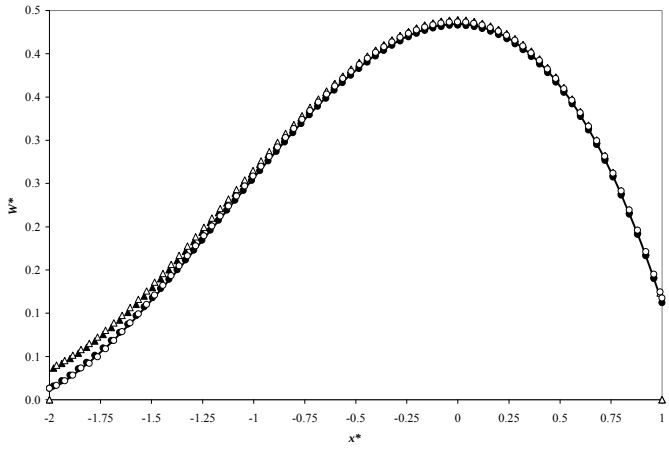

Figure 6: Equilateral triangular section - dimensionless velocity along the symmetry axis (y* = 0): comparison between analytical results (—), S/6 MW (○), S/6 LPBS (Δ), S/2 MW (●), S/2 LPBS(▲) simulations for *Kn* = 0.075.

As a conclusion, the LPBS method proposed in Fluent can be used with a good accuracy only for low Knudsen numbers. For Knudsen numbers higher than 0.025, this method overestimates slip at the wall near the angles, which leads to an overestimation of the flow rate.

The MW method proposed in this paper has been shown to be very accurate whatever the Knudsen number in the range $[10^{-3};10^{-1}]$ and gives very similar results when using or not symmetries of the section: for an equilateral triangular section, deviations from the analytical solution were always lower than 0.2 %. This method proved to be accurate even in acute angles, and consequently could be employed with a good precision for slip flow simulations with first order boundary conditions on more complex channels geometries. Moreover, it permits to implement various slip boundary conditions types with different orders or mean free path definitions, which is not allowed in the LPBS method.

3. SLIP FLOW IN ISOSCELES TRIANGULAR AND TRAPEZOIDAL SECTIONS

3.1 Numerical simulation

Slip flow through realistic microchannels, with isosceles triangular and trapezoidal sections which could be made by anisotropic wet etching on silicon wafers, are now investigated. Their geometries are shown in figure 7. Dimensions are normalized by a reference length *L* as for the equilateral triangular section. According to the etching time, the etching can be limited in the x-direction, leading to a trapezoidal section. For longer-term etching, the section is an isosceles triangle. For a silicon wafer with a $\langle 100 \rangle$ surface orientation, the angle $\beta = 54.74°$.

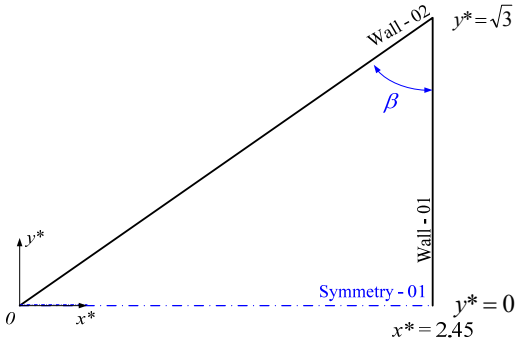

Figure 7a: Isosceles triangular section with $D_h^* = 1.773$

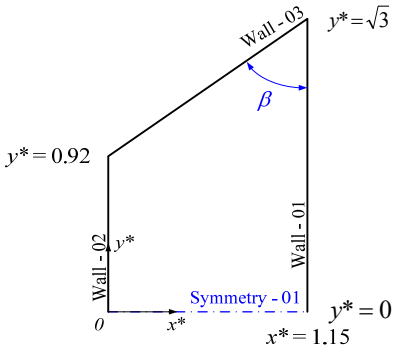

Figure 7b: trapezoidal section with $D_h^* = 1.502$; $\beta = 54.74°$

Grids with quadrilateral cells are generated with Gambit. The operating conditions are the same as those used for the equilateral triangular section.

3.2 Results and discussion

Table 4 shows dimensionless mass flow rates through microchannels with equilateral triangular, isosceles and trapezoidal sections both for MW and LPBS boundary conditions for the same value of *Kn'*. $Kn' = \lambda / (\sqrt{3}\, L) = 0.0866$ is based on the section half width in the 3 cases. As observed in section 2, the LPBS method gives a higher mass flow rate than the MW method whatever the Knudsen number. This is due again to the overestimation of the velocity by the LPBS method in zones presenting angles, as shown in figures 8, 9 and 10.

Table 4: Comparison of mass flow rates through equilateral triangular, isosceles rectangular and trapezoidal sections for the same length of wall-01 ($Kn' = \lambda \Big/ \left(\sqrt{3}\, L \right) = 0.0866$ in the 3 cases)

	Kn	$\dot{m}$ *			
		Fluent 1st iteration	Fluent 2nd iteration	Fluent 3rd iteration	Fluent LPBS
Equilateral triangular section	0.075	1.600	1.584	1.585	1.604
Isosceles triangular section	0.084	1.668	1.650	1.653	1.674
Trapezoidal section	0.100	1.861	1.831	1.843	1.866

Figure 8 presents the velocity profiles obtained by both methods along the symmetry axis of an isosceles triangular section. No difference can be observed between both profiles near the base of the triangular section, where the symmetry axis is perpendicular to the wall, but the deviation is increasing when approaching the other wall which forms an acute angle with the symmetry axis. The same phenomena can be observed in figure 9 along the walls 01 and 02 of a trapezoidal section: no significant discrepancy between both methods near the symmetry axis, but increasing differences when approaching the angular zones. Moreover, figure 10 shows that for a trapezoidal section the two methods lead to the same velocity profile on the symmetry plane which is normal to the two walls. On the other hand, discrepancies are very sensitive along the wall between the two angles (figure 11), and it can observed that the more acute the angle, the more the deviation of LPBS method with MW method. In the same way, this deviation has an influence farther away from the angle when it is more acute (case of angle at $x^* = 1.15$ to be compared with the angle at $x^* = 0$). This observation is confirmed by data plotted in figure 9.

Finally, the values of Poiseuille number calculated from the product of the friction factor *f* and the Reynolds number *Re* for both methods have been compared in Table 5 to the numerical values from Morini *et al.* [16]. All results are in excellent agreement but MW results are closer to Morini's ones. However, additional comparisons on other geometrical configurations should be performed in future work to confirm this analysis.

Table 5: Product of friction factor and Reynolds number: comparison with the results from [16], for $\beta_{TZ} = 0.2$ and $\gamma_{TZ} = 0.156$ (β_{TZ} = height / 2 x larger of wall02, γ_{TZ} = height / 2 x larger of wall01).

β_{TZ}	γ_{TZ}		$Kn = 0$	$Kn = 0.1$	
			$f\,Re$	$f\,Re$ - MW	$f\,Re$ - LPBS
0.200	0.156	Morini *et al.*	18.650	9.267	
		present calculations	18.635	9.266	9.204
		deviation (%)	-0.081	-0.015	-0.684

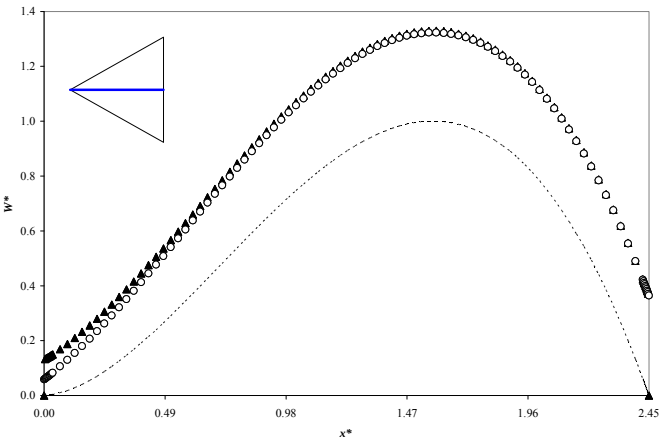

Figure 8: Isosceles triangular section, dimensionless velocity along the symmetry axis ($y^* = 0$); comparison between no slip (--), MW (O) and LPBS (Δ) simulations for $Kn' = 0.0866$

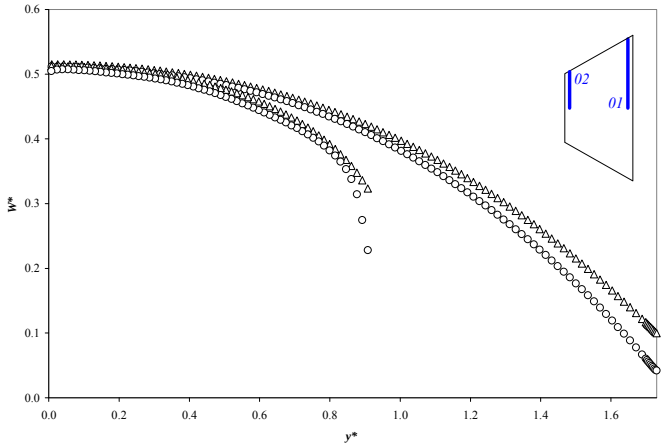

Figure 9: Trapezoidal section, dimensionless velocity at cells center near the walls ($x^* = 0$, $x^* = 1.15$); comparison between MW (O) and LPBS (Δ) simulations for $Kn' = 0.0866$

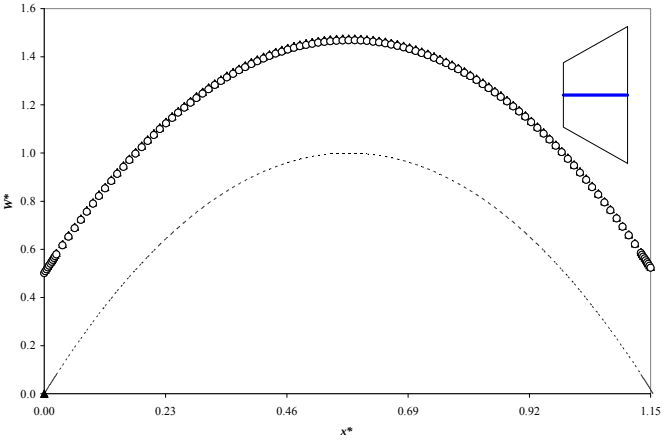

Figure 10: Trapezoidal section, dimensionless velocity along the symmetry axis ($y^* = 0$); comparison between no slip (--), MW (O) and LPBS (Δ) simulations for $Kn' = 0.0866$

4. CONCLUSION AND PERSPECTIVES

Rarefied gas flows in microchannels with triangular or trapezoidal sections have been simulated using Fluent CFD code. Two methods were tested for first order slip boundary conditions implementation: the LPBS method currently developed in Fluent and the MW method proposed in this article. Mass flow rates and velocity profiles were calculated from MW and LPBS methods and compared for validation to the analytical solution for equilateral triangular sections, before applying them to isosceles and trapezoidal sections. This investigation pointed out the LPBS limitations:

(l) Only Maxwell's slip models are allowed for slip flow simulation with the LPBS method. No other slip coefficient or higher order slip models (e.g. second order boundary conditions proposed by Deissler [8]) can be used with this method.

(2) The mean free path used by the LPBS method is necessarily calculated from equation 13. Nevertheless, a fictitious adjustment of the Lennard-Jones length value allows modifying the expression of λ by a multiplier coefficient.

(3) LPBS method does not calculate slip velocity exactly at the wall. Only the velocity at cell centers near the wall is available.

In addition to these limitations, important slip velocity deviations from analytical solutions were found near the angles. These local deviations increase with Knudsen number and can reach 100% and more in some cases, leading to significant errors on mass flow rate estimation. They are particularly sensitive in acute angles.

On the contrary, in the MW method, various kinds of slip boundary conditions and diverse definitions of the mean free path may be used. The very good agreement between the numerical results and the analytical ones (less than 0.2 % deviation for Knudsen numbers up to 0.075 in the case of an equilateral triangular section) supports the use of this method for numerical simulations in the slip flow regime.
Future work will include:

- Implementation of second order boundary conditions for simulating higher Knudsen numbers flows;
- 3D simulations in more complex geometries;
- Comparison with simulated data using near-wall scaling function for describing the non-linear stress-strain relationship within the Knudsen layer [2], [17].

5. NOMENCLATURE

A_α	dimensionless slip coefficient without Maxwell's reflection term
A^*	dimensionless constant of analytical slip flow equation in trapezoidal section
B^*	dimensionless constant of analytical slip flow equation in trapezoidal section
D_h	hydraulic diameter
Kn	Knudsen number
k_B	Boltzman constant (1.38066E-23 JK^{-1})
L	characteristic length
$\dot{m}$	mass flow rate
$\dot{m}_{NS}$	no-slip mass flow rate
$\dot{m}^*$	non - dimensional mass flow rate
n	normal direction
P	pressure
T	temperature
W	streamwise velocity
W_s	flow velocity at the wall
W_{slip}	slip velocity
W_w	velocity of the wall
W^*	dimensionless velocity
x	widthwise coordinate
y	depthwise coordinate
z	streamwise coordinate
α	slip coefficient with mean free path of the molecules and Maxwell's reflection term
α^*	dimensionless slip coefficient with mean free path of the molecules and Maxwell's reflection term
β	base angle
β_{TZ}	aspect ratio of trapezoidal section
γ_{TZ}	aspect ratio of trapezoidal section
λ	mean free path of the molecules
μ	dynamic viscosity of the gas
σ	Lennard-Jones characteristic length of the gas
σ_v	tangential momentum accommodation coefficient

6. REFERENCES

1. G. E. Karniadakis and A. Beskok, Microflows: fundamentals and simulation, Springer-Verlag, New York, 2002.
2. D. A. Lockerby, J. M. Reese and M. A. Gallis, Capturing the Knudsen layer in continuum-fluid models of nonequilibrium gas flows, *AIAA Journal*, vol. 43(6), pp. 1391-1393, 2005.
3. S. Colin, P. Lalonde and R. Caen, Validation of a second-order slip flow model in rectangular microchannels, *Heat Transfer Engineering*, vol. 25(3), pp. 23-30, 2004.
4. J. Maurer, P. Tabeling, P. Joseph and H. Willaime, Second-order slip laws in microchannels for helium and nitrogen, *Physics of Fluids*, vol. 15(9), pp. 2613-2621, 2003.
5. J. C. Maxwell, On stresses in rarefied gases arising from inequalities of temperature, *Philosophical Transactions of the Royal Society*, vol. 170, pp. 231-256, 1879.
6. C. Cercignani, R. Illner and M. Pulvirenti, The mathematical theory of dilute gases, Springer-Verlag, New-York, 1994.
7. S. Chapman and T. G. Cowling, The mathematical theory of non-uniform gases, University Press, Cambridge, 1952.
8. R. G. Deissler, An analysis of second-order slip flow and temperature-jump boundary conditions for rarefied gases, *International Journal of Heat and Mass Transfer*, vol. 7, pp. 681-694, 1964.
9. Y.-T. Hsia and G. A. Domoto, An experimental investigation of molecular rarefaction effects in gas lubricated bearings at ultra-low clearances, *Journal of Lubrication Technology*, vol. 105, pp. 120-130, 1983.
10. Y. Mitsuya, Modified Reynolds equation for ultra-thin film gas lubrication using 1,5-order slip-flow model and considering surface accommodation coefficient, *Journal of Tribology*, vol. 115, pp. 289-294, 1993.
11. A. K. Sreekanth, Slip flow through long circular tubes, 6th International Symposium on Rarefied Gas

Dynamics, L. Trilling and H. Y. Wachman, eds., Academic Press, New York, pp. 667-680, 1969.
12. S. Colin, Chapter 2: Single-phase gas flow in microchannels, Heat Transfer and Fluid Flow in Minichannels and Microchannels, S. G. Kandlikar, S. Garimella, D. Li, S. Colin, and M. King, eds., Elsevier, pp. 9-86, 2006.
13. W. A. Ebert and E. M. Sparrow, Slip flow in rectangular and annular ducts, *Journal of Basic Engineering*, vol. 87, pp. 1018-1024, 1965.
14. Aubert and S. Colin, High-order boundary conditions for gaseous flows in rectangular microchannels, *Microscale Thermophysical Engineering*, vol. 5(1), pp. 41-54, 2001.
15. C. Y. Wang, Slip flow in a triangular duct - an exact solution, *ZAMM - Journal of Applied Mathematics and Mechanics*, vol. 83(9), pp. 629-631, 2003.
16. G. L. Morini, M. Spiga and P. Tartarini, The rarefaction effect on the friction factor gas flow in microchannels, *Superlattices and Microstructures*, vol. 35(3-6), pp. 587-599, 2004.
17. T. J. Scanlon, J. M. Reese and L. O'Hare, A procedure for calculating wall distance in arbitrary microchannel geometries, Proceedings of 4th International Conference on Nanochannels, Microchannels and Minichannels, ASME, Limerick, Ireland, ICNMM2006-96037/1-6, 2006.